International Journal of Microwave and Wireless Technologies, 2015, 7(5), 597–603.
doi:10.1017/S1759078715001233

RESEARCH PAPER

A super-resolution polarimetric wavefront extraction algorithm for UWB-radar under massive interference conditions

DILYAN DAMYANOV[1], RAHMI SALMAN[2], THORSTEN SCHULTZE[1] AND INGOLF WILLMS[1]

To provide short-range super-resolution ultra-wideband (UWB) radar under multi-scattering conditions, a superior wavefront extraction algorithm is proposed in this paper. Conventional correlation-based pulse separation methods based on SAGE, CLEAN or the previously introduced superior dynamic correlation method (DCM) are revised, validated, and compared. In this paper, the DCM is improved significantly by applying the Pauli scattering matrix decomposition onto the radar data. This novel wavefront extraction algorithm is called polarimetric dynamic correlation method (PDCM) and is suitable to resolve several overlapping pulses, which consist of both strong echoes and weak echoes which are masked by the strong ones. The performance of the PDCM and the comparison with alternative algorithms is carried out by a subsequent feature extraction algorithm for visual verification. Experimental validations are performed with two complex test objects, a maximum length sequence radar device (4.5–13.5 GHz) and compact dual-polarized UWB antennas.

Keywords: Radar signal processing and system modeling, Radar applications

Received 30 October 2014; Revised 1 July 2015; Accepted 2 July 2015; first published online 29 July 2015

I. INTRODUCTION

Radar systems equipped with ultra-wideband (UWB) sensors are attractive for detection and imaging applications in emergency situations. Compared with other sensing technologies such as continuous wave (CW)-radar, optical or infrared systems UWB radar does not need a visual line-of-sight (LOS) making it suitable for smoke and dust-filled emergency scenarios. The fine time resolution due to the huge bandwidth provides accuracy and resolution in the millimeter range. Thus, a certain degree of multipath immunity is provided. However, the separation of multiple wavefronts under severe interference conditions with no *a priori* information still keeps a challenging issue in the field of super-resolution applications. Classical correlation-based algorithms which are based on iterative cancellation of extracted wavefronts [1] show a poor performance when the pulses overlap almost the whole pulse duration. In [2] the superior dynamic correlation method (DCM) algorithm has been proposed which performs the correlation operation with a set of synthetic waveform patterns. However, in scenarios where strong echoes (e.g. induced by double-bounce reflection) interfere with weak diffuse scattering contributions also, the DCM performs not so well. In this case, weak echoes are masked by the strong ones and the original evolution of the signal cannot be recovered anymore.

In this paper, the DCM is drastically improved by the exploitation of polarimetric diversity gain. This is foremost achieved by applying the Pauli scattering matrix decomposition onto the polarimetric radar data. Hence, the data are separated in a double-bounce and a single-bounce signature. A concluding optimization algorithm is proposed which exploits the time evolution history in slow time domain.

II. HARDWARE SETUP AND OBJECT UNDER TEST

Several methods exist for the generation of UWB-pulses. The radar system used for this paper consists of a UWB maximum length sequence (M-sequence) generator [3] with an operating band of DC-4.5 GHz. Higher time resolution is achieved by an additional quadrature modulator, which operates with a carrier frequency of 9 GHz and doubles the bandwidth to 4.5–13.5 GHz. Two dual-polarized antennas are mounted in a bistatic configuration where the Tx and Rx are separated by a 25 cm distance. The antennas are dual-polarized antennas and hence consist of two substrates which are connected orthogonally to each other. On each substrate an array of two vivaldi antennas are designed and the whole construction is embedded in Teflon [4]. Two objects are considered for the experimental investigation of the described wavefront extraction algorithms from Section III. The objects are 1 m high and photographs of the objects and their cross-section are shown in Fig. 1.

[1]University of Duisburg-Essen, Chair of Communication Systems, Bismarckstrasse 81, 47057 Duisburg, Germany. Phone: +49 203 379 4408
[2]HF Systems Engineering GmbH & Co. KG, Heinrich-Hertz-Straße 6, 34123 Kassel, Germany
Corresponding author:
D. Damyanov
Email: dilyan.damyanov@uni-due.de

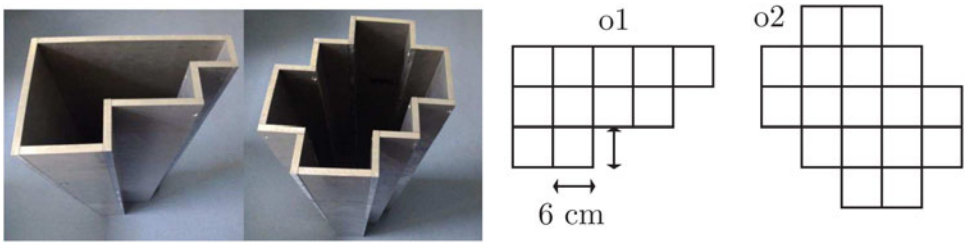

Fig. 1. Objects under test.

The object under test is positioned on a rotatable table driven by an accurate step motor. The objects exhibit a high number of dihedrals and edges resulting in richly interfering conditions. For the measurement scenario the object under test is placed in front of the sensors at a distance of 1 m, simulating an indoor scenario, where space is limited and the objects are positioned in the near-field of the antennas. In Fig. 2, a schematic of the measurement setup is shown. A measurement of the object under test is then performed using a 0.5° grid resulting in 720 impulse responses $m(t)$. The pulses are then combined to a set of measurements which are widely known as B-scan or a radargram. The radargrams are gray scale coded where the intensity describes the strength of the electromagnetic field.

III. WAVEFRONT EXTRACTION

A major topic in super-resolution radars is the correct extraction of wavefronts from the object's radargram. For objects which exhibit a single reflection per impulse response wavefront extraction can be performed quite straightforward. But for the case when multiple scatterers are observed things become challenging. Multiple reflections are obtained which are often overlapped making the correct detection of the reflected echoes more complex.

In the following, two wavefront extraction algorithms based on the matched filter correlation principle are briefly discussed and compared. Afterwards, a more efficient and higher performing algorithm is derived. All algorithms are applied to the same radar data of the object under test.

The results are verified with an imaging algorithm based on [5]. The algorithm uses fuzzy-logic principles for an accurate estimation of the angle-of-arrival and maps the observed range to a target point. Experimental validation of the algorithm in [5] has proven the capability of the algorithm for multi-scattering conditions.

A) Classical correlation method (CCM)

The algorithm discussed here is based on the algorithm proposed in [1]. The idea of this algorithm is to extract echoes iteratively by the evaluation of the normalized cross-correlation function with an *a priori* obtained reference pulse using a metal plate as described in [1]. After the wavefront is extracted, a subtraction between the measurement under test (MUT) and the scaled reference pulse is performed that provides the remaining part of the MUT for the next iterations. These steps are repeated until a fixed termination condition is fulfilled. Typical termination conditions are:

- Fixed number of found reflections or iterations;
- Minimum value for the maximum cross-correlation coefficient;
- Evaluation of the remaining energy of the MUT after subtraction.

These fixed termination conditions do not adapt to scenarios which exhibit various energy levels due to strong and weak echoes. Furthermore, the subtraction of a reference pulse from a MUT that exhibits a superposition of several pulses also removes information which is needed for the next iterations. Finally, the cross-correlation between a single reference pulse and a superposition of two or more pulses has marginal values due to the constructive or destructive interference of the pulses. Hence, the CCM cannot resolve richly interfered pulses.

The results of the CCM applied to the radargrams of the objects under test are shown in Fig. 3 and the extracted features in Fig. 4.

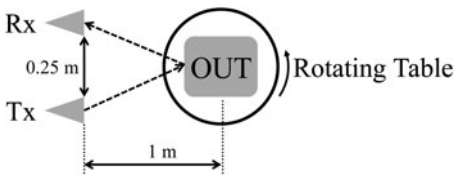

Fig. 2. Measurement setup.

B) DCM

The second wavefront extraction algorithm discussed in this paper is the DCM proposed in [2]. The algorithm is based on the CCM where a cross-correlation between a reference pulse and the MUT is performed. However, in the DCM a set of synthetic wavefront patterns consisting of a superposition of two differently delayed reference pulses is used as a new synthetic reference for the correlation with the MUT. From the correlation between the MUT and the synthetic reference two wavefronts are extracted, instead of a single wavefront as with the CCM. Subsequently, the relative distance between the two wavefronts is compared with a given constant. The constant used here is λ_c, where λ_c is the wavelength at the center frequency. Afterwards, a decision for the discarding of the second wavefront is made. The extracted wavefronts are then windowed from the MUT. The method is iterated until a termination condition is fulfilled. As a termination condition in the DCM a dynamic power detector is employed as described in [2].

Due to the dynamic termination condition and the new synthetic reference pulse the DCM proved to be a powerful tool for the extraction of wavefronts from richly interfered pulses. However, due to the complexity of the investigated objects some of the echoes can not be precisely detected

https://doi.org/10.1017/S1759078715001233 Published online by Cambridge University Press

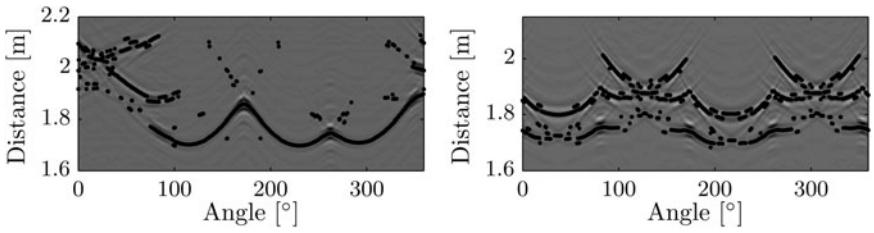

Fig. 3. Extracted wavefronts of objects 01 (left) and 02 (right) by the CCM.

because of the interference of multiple echoes with very different energy levels.

In Fig. 5, the output of the DCM applied to the same radar data of both objects is highlighted, the processed image is shown in Fig. 6.

C) Proposed polarimetric dynamic correlation method (PDCM)

The new proposed wavefront extraction algorithm is designed to merge the following advantages of the previously mentioned DCM and the theory of radar polarimetry:

- Cross-correlation with a set of a synthetic reference pattern;
- Dynamic termination condition;
- Separation of weak single-bounce scattering and strong double-bounce scattering.

According to [6] the fully polarimetric scattering behavior can be expressed by the 2 × 2 scattering matrix

$$[S(f)] = |S(f)|\begin{bmatrix} S_{HH} & S_{HV} \\ S_{VH} & S_{VV} \end{bmatrix}, \tag{1}$$

where $|S(f)|$ is a weighting factor, S_{HV}, S_{VH} the cross-polarization coefficients, and S_{HH}, S_{VV} the co-polarization coefficients, respectively. Furthermore, the single- and double-bounce calibration targets (flat plate and dihedral, respectively) exhibit the following simplified scattering matrices:

$$\begin{aligned} [S_{single}(f)] &= |S_{single}(f)|\begin{bmatrix} S_{HH} & S_{HV} \\ S_{VH} & S_{VV} \end{bmatrix}, \\ [S_{double}(f)] &= |S_{double}(f)|\begin{bmatrix} S_{HH} & S_{HV} \\ S_{VH} & -S_{VV} \end{bmatrix}, \end{aligned} \tag{2}$$

where $[S_{single}(f)]$ is the scattering matrix for single bounce and $[S_{doulble}(f)]$ for double bounce. Although the contribution from the cross-polarization is not zero in real life measurements, here they are neglected as only the co-polarization contribution is measured. Furthermore, the ratio between S_{HH}/S_{VV} can be determined by calibration measurements of metal plate and perfect dihedral. Thus, the scattering matrix from (2) can be rewritten as,

$$\begin{aligned} [S_{single}(f)] &= |S_{single}(f)|\begin{bmatrix} 1 & 0 \\ 0 & 1 \end{bmatrix}, \\ [S_{double}(f)] &= |S_{double}(f)|\begin{bmatrix} 1 & 0 \\ 0 & -1 \end{bmatrix}. \end{aligned} \tag{3}$$

From equation (3) two new radargrams can be obtained by combination of the two scattering matrices as

$$\begin{aligned} m_{MUT,S}(t) &= m_{MUT,HH}(t) + m_{MUT,VV}(t), \\ m_{MUT,D}(t) &= m_{MUT,HH}(t) - m_{MUT,VV}(t), \end{aligned} \tag{4}$$

where $m_{MUT,HH}(t)$ is the MUT obtained from a horizontally polarized wave and $m_{MUT,VV}(t)$ is the MUT obtained from a vertically polarized wave for the same position of the transmitter and receiver antennas. Thus, two new measurements of the object under test are obtained, where $m_{MUT,S}(t)$ exhibits only the contributions from single-bounce scatterers and $m_{MUT,D}(t)$ exhibits reflections only from double-bounce scatterers. In Fig. 7, two sample measurements from object 01 $m_{MUT,HH}(t)$ and $m_{MUT,VV}(t)$, the resulting single bounce $m_{MUT,S}(t)$, and double bounce $m_{MUT,D}(t)$ measurements and the positions of the reflections for the four measurements are shown.

From the figure, it can be seen that in this example after combining the impulse responses $m_{MUT,VV}(t)$ and $m_{MUT,HH}(t)$ to $m_{MUT,S}(t)$ and $m_{MUT,D}(t)$, three echoes can be extracted for the single-bounce scatterers and two echoes from the impulse response for the double-bounce scatterers so altogether five echoes can be extracted. This is not the

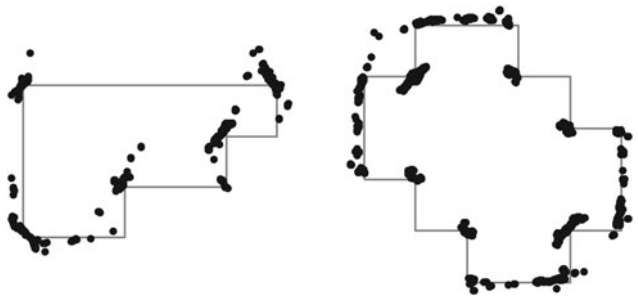

Fig. 4. Extracted features of objects 01 (left) and 02 (right) by the CCM.

https://doi.org/10.1017/S1759078715001233 Published online by Cambridge University Press

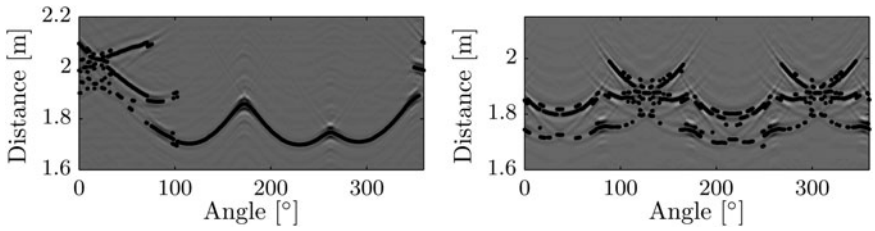

Fig. 5. Extracted wavefronts of objects 01 (left) and 02 (right) by the DCM.

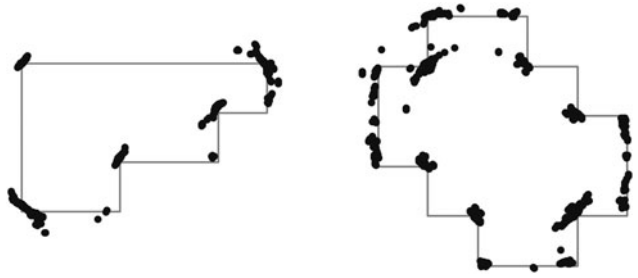

Fig. 6. Extracted features of objects 01 (left) and 02 (right) by the DCM.

case if the two impulse responses $m_{MUT,VV}(t)$ and $m_{MUT,HH}(t)$ are examined separately. Owing to interference from the single-bounce and the double-bounce scatterers, a maximum of four reflections can be extracted for either two impulse responses $m_{MUT,VV}(t)$ and $m_{MUT,HH}(t)$. Thus, equation (4) is performed for each MUT resulting in two separate radargrams. The first radargram is obtained for the single-bounce contributions only and for the second radargram only the double-bounce contributions are taken into account as shown in Fig. 8. The wavefronts from the two radargrams can then be extracted separately by applying the following algorithm to the two radargrams.

Let $m_{ref}(t)$ be an *a priori* measured reference pulse. The point in time of the maximal absolute amplitude is found as

$$t_{ref,max} = \arg\max_t(|m_{ref}(t)|). \tag{5}$$

The reference pulse is then circularly shifted with $t_{ref,\ max}$ resulting in

$$m_{ref,shift}(t) = m_{ref}(t + t_{ref,max}). \tag{6}$$

The shifted reference pulse $m_{ref,shift}(t)$ is then windowed as

$$m^w_{ref,shift}(t) = m_{ref,shift}(t)\mathrm{rect}\left(\frac{t}{T_w}\right), \tag{7}$$

where $T_w = 1,5\lambda_c$, with λ_c the wavelength at the carrier frequency. The reference pulse of equation (7) is further used for the design of a new set of synthetic reference pulses as

$$m_{ref,syn}(t, \tau_{syn}) = m^w_{ref,shift}(t) + m^w_{ref,shift}(t - \tau_{syn}), \tag{8}$$

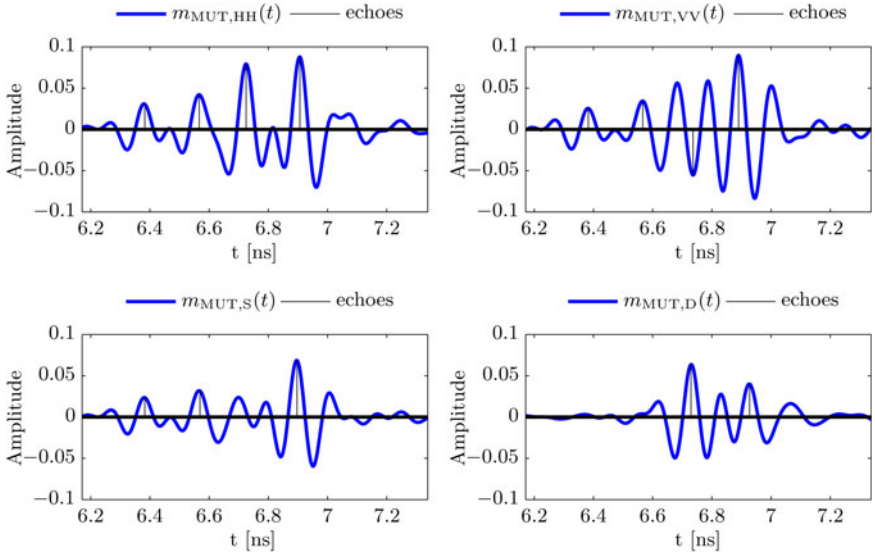

Fig. 7. Sample measurements and the positions of the echoes.

https://doi.org/10.1017/S1759078715001233 Published online by Cambridge University Press

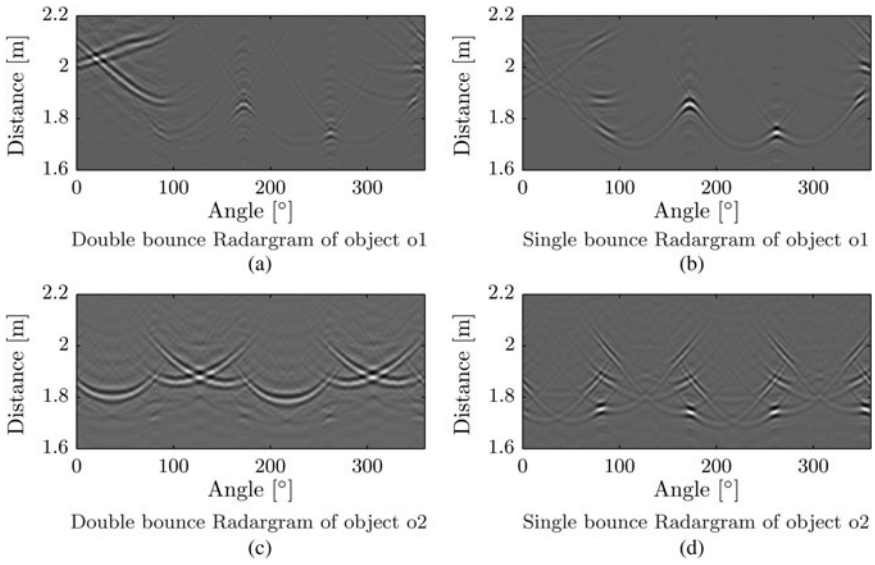

Fig. 8. Single- and double-bounce radargrams of objects o1 and o2.

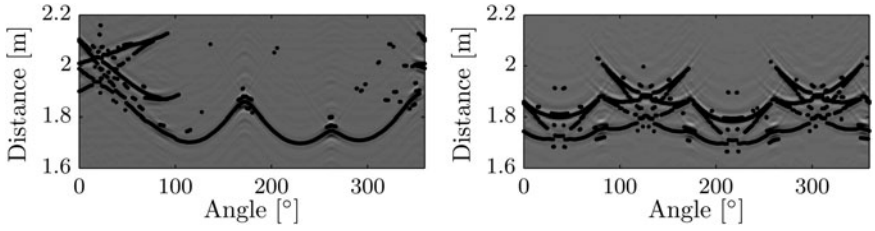

Fig. 9. Extracted wavefronts of objects o1 (left) and o2 (right) by the PDCM.

where τ_{syn} is the delay time of the second reference pulse. The new set of synthetic reference pulses exhibits every possible interference of two pulses, thus interference effects are respected. For the wavefront extraction with the set of synthetic reference pulses a two-dimensional normalized cross-correlation operation

$$R_{m_{MUT}m_{ref,syn}}(t, \tau_{syn}) = \frac{\int_{-\infty}^{\infty} m_{MUT}(t) m_{ref,syn}(t-\tau, \tau_{syn}) dt}{\| m_{MUT}(t)\|_2 \, \| m_{ref,syn}(t, \tau_{syn})\|_2} \quad (9)$$

is performed, where m_{MUT} is the impulse response of the MUT for the single- or double-bounce scatterers. The cross-correlation from (9) depends both on the delay parameter τ and the delay time τ_{syn} of the synthetic reference pulses. Thus, the highest degree of similarity is obtained from the absolute maximum of the correlation matrix $R_{m_{MUT}m_{ref,syn}}$ which yields

$$\tau_{max}, \tau_{syn_{max}} = \arg\max_{\tau, \tau_{syn}} (R_{m_{MUT}m_{ref,syn}}(t, \tau_{syn})). \quad (10)$$

The positions in time of the two extracted wavefronts are respectively,

- First wavefront at τ_{max}.
- Second wavefront at $\tau_{max} + \tau_{syn_{max}}$.

Furthermore, if the value of $\tau_{syn_{max}}$ is smaller than λ_c the second wavefront is discarded. In the next step, a recovered pulse is obtained as

$$m_{rec}(t) = m_{ref,shift}(t-\tau_{max}) + m_{ref,shift}(t-\tau_{max}-\tau_{syn_{max}}). \quad (11)$$

The recovered pulse is designed to exhibit two wavefronts at the extracted time positions from the MUT. The energy levels of the wavefronts from the recovered pulse are then normalized with the energy levels of the wavefronts from the MUT as

$$m_{rec,norm}(t) = m_{rec}(t) \cdot \frac{\| m_{MUT}(t)w(t)\|_2}{\| m_{rec}(t)w(t)\|_2}, \quad (12)$$

where $w(t)$ is a windowing function according to

$$w(t) = \begin{cases} 1 & \text{if } m^w_{ref,shift}(t-\tau_{max}) \neq 0, \\ 1 & \text{if } m^w_{ref,shift}(t-\tau_{max}-\tau_{syn_{max}}) \neq 0, \\ 0 & \text{else.} \end{cases} \quad (13)$$

The normalized recovered pulse is then used in an energy comparator. If the energy of the MUT is greater than the energy of the recovered pulse, the algorithm is iterated with

https://doi.org/10.1017/S1759078715001233 Published online by Cambridge University Press

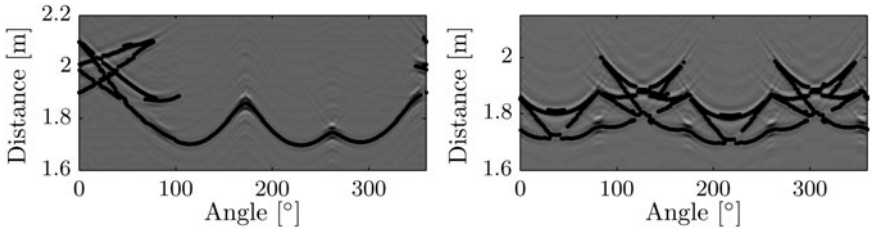

Fig. 10. Extracted wavefronts of objects 01 (left) and 02 (right) by the PDCM after optimization.

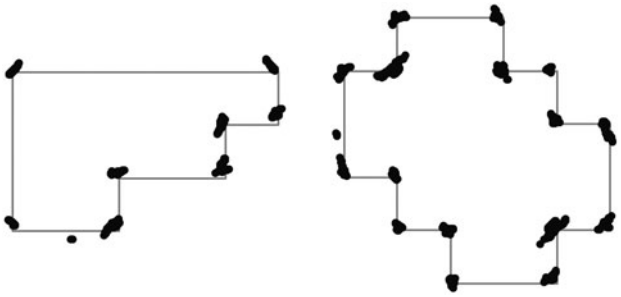

Fig. 11. Extracted features of objects 01 (left) and 02 (right) by the PDCM.

the new MUT pulse

$$m_{MUT}(t) = m_{MUT}(t)(1 - w(t)). \quad (14)$$

The algorithm results in two sets of wavefronts for the strong double-bounce scatterers and for the weak single-bounce scatterers. The extracted wavefronts from the single- and double-bounce impulse responses are then merged together for each antennas position. In Fig. 9, the results for objects 01 and 02 are shown.

The merged wavefronts then are optimized using a post-processing algorithm in four steps:

1. Wavefronts are clustered depending on their relative distance in both slow and fast times.
2. The resulting clusters are approximated using a polynomial curve-fitting algorithm.
3. Gaps in the wavefronts clusters are detected and compensated using the approximated polynomials.
4. Clusters with less than a minimum number of wavefront points are discarded.

In Fig. 10, the output of the new proposed PDCM applied to the two objects under test are shown, the processed images are shown in Fig. 11.

IV. EVALUATION

A numerical accuracy evaluation of the wavefront extraction algorithms shall be provided in this section. An iso-artifact quantity

$$\tilde{a}_n = \min_{\vec{\mathbf{P}}_{\text{real}}} \| \vec{\mathbf{P}}^{\,n}_{\text{sc}} - \vec{\mathbf{P}}_{\text{real}} \| \text{ with } n = 1, \ldots, N; \quad (15)$$

is defined, where $\vec{\mathbf{P}}^{\,n}_{\text{sc}}$ are the approximated target-scattering centers coordinates, calculated using [5] and the wavefronts extracted from presented algorithms. Furthermore, $\vec{\mathbf{P}}_{\text{real}}$ are the true target-scattering centers coordinates. In Fig. 12, the cumulative distribution function $F_{\tilde{a}_n}(\tilde{a}_n)$ for the three wavefront extraction algorithms are shown for objects 01 and 02, respectively.

From the figure, it can be seen that in the case of object 01 the proposed algorithm exhibits 99% of all target points with a translative error $\tilde{a}$ of less than or equal to $0.6\lambda_c$, whereas the value falls to 94% for the DCM and 92% for the classical correlation algorithm. Furthermore, the number of extracted wavefronts (wf) with the proposed algorithm is 1342, where 946 are extracted using the DCM and 1048 with the classical correlation algorithm resulting in an 30% increase of the extracted wavefronts by employing the proposed method. In the case of object 02, the percentage of the target points with a translative error of less than $\tilde{a} = 0.6\lambda_c$ is 100% for the proposed method, 90% for the DCM and 89% for the classical correlation. Moreover, the number of extracted wavefronts for object 02 using PDCM is double the number of extracted wavefronts with the DCM and 90% more extracted wavefronts with the CCM.

V. CONCLUSION

In this paper, two wavefront extraction algorithms based on the matched filter correlation principle are briefly described. Their performance was analyzed using the radar data from two complex objects. From the gathered information the drawbacks of DCM are analyzed and a new optimized wavefront extraction method called PDCM is proposed. The new method exhibits the advantages of the DCM and compensates its drawbacks by employing the theory of radar polarimetry

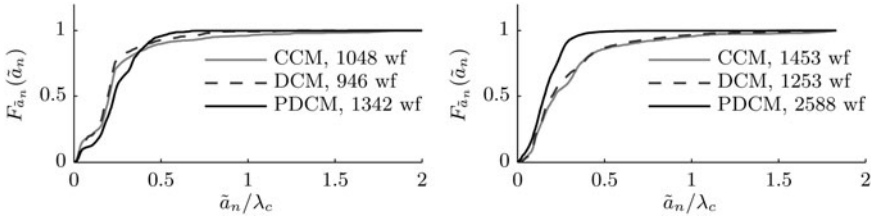

Fig. 12. Evaluation using objects 01 (left) and 02 (right).

https://doi.org/10.1017/S1759078715001233 Published online by Cambridge University Press

and a post-processing algorithm based on polynomial fitting. The PDCM separates the information of single- and double-bounce contributions in two different radargrams, which enables the detection of weak reflections previously masked by the strong ones. The PDCM terminates adaptively and exploits the time evolution history in slow time domain.

REFERENCES

[1] Hantscher, S.; Etzlinger, B.; Reisenzahn, A.; Diskus, C.: A wave front extraction algorithm for high-resolution pulse based radar systems, in IEEE Int. Conf. Ultra-Wideband (ICUWB), 24–26 September 2007.

[2] Salman, R.; Willms, I.: Joint efficiency and performance enhancement of wavefront extraction algorithms for short-range super-resolution UWB radar, in the Seventh German Microwave Conf. (GeMiC), 12–14 March 2012.

[3] Sachs, J.; Herrmann, R.; Kmec, M.; Helbig, M.; Schilling, K.: Recent advances and applications of m-sequence based ultra-wideband sensors, in IEEE Int. Conf. Ultra-Wideband, 24–26 September 2007.

[4] Reichardt, L.; Kowalewski, J.; Zwirello, L.; Zwick, T.: Compact, Teflon embedded, dual-polarized ultra wideband (UWB) antenna, in Int. Symp. Antennas and Propagation Society (APSURSI), 8–14 July 2012.

[5] Salman, R.; Willms, I.: 3D UWB radar super-resolution imaging for complex objects with discontinuous wavefronts, in IEEE Int. Conf. Ultra-Wideband, 14–16 September 2011.

[6] Salman, R.; Willms, I.; Reichardt, L.; Wiesbeck, W.: On polarization diversity gain in short range UWB-radar object imaging, in IEEE Int. Conf. Ultra-Wideband (ICUWB), 17–20 September 2012.

Dilyan Damyanov received his Masters degree in Communication Engineering from the University of Duisburg-Essen in 2014 and has been working at the University of Duisburg-Essen since 2014. His main research interest is broadband radar sensors for fire and security applications and especially radar localization, wavefront extraction, and imaging techniques.

Rahmi Salman received his Dipl.-Ing. (M.S.E.E.) from the Technical University of Dortmund in 2007 and received his Dr.-Ing. (Ph.D.E.E.) degree with distinction from the University of Duisburg-Essen in 2014. Since 2014 he has been with the Radar and Microwave company HF Systems Engineering GmbH & Co. KG in Kassel (Germany) of which he is also the co-founder. His main research interests are ultra-wideband radar sensors, radar signal processing as well as radar design. He published more than 30 papers in this field of which two were awarded with best paper awards.

Thorsten Schultze received his Diploma degree in Electrical Engineering from the University of Duisburg-Essen in 2003 and in 2010 he received his Ph.D. degree also in Electrical Engineering. He now works as an Academic Senior Councillor (akademischer Oberrat) at the Chair of Communication Systems at the University of Duisburg-Essen. His main research interests are automatic fire detection technologies and broadband radar sensors for fire and security applications.

Ingolf Willms received his Diploma degree in Electrical Engineering from the RWTH Aachen University in 1976 and received his Ph.D. degree also in Electrical Engineering in 1983. Since 1990 he has been with the Chair of Communication Engineering at the University Duisburg-Essen. His main research interests are automatic fire detection technologies and especially broadband radar sensors for fire and security applications.

https://doi.org/10.1017/S1759078715001233 Published online by Cambridge University Press